# Nonlinear Dynamic Analysis of Annular FG Porous Sandwich Plates Reinforced by Graphene Platelets

## H. Jafary, M.E. Golmakani *

*Department of Mechanical Engineering, Mashhad Branch, Islamic Azad University, Mashhad, Iran*

## KEYWORDS

## ABSTRACT

In this paper, the nonlinear dynamic analysis of porous annular sandwich plates reinforced with graphene platelets (GPLs) under different boundary conditions is investigated. The Gaussian Random Field (GRF) alongside with Halpin-Tsai micromechanics model are used for the variational Poisson's ratio and effective material property of the GPLs which are distributed in two forms of symmetric and non-symmetric patterns with different porosity dispersion models. Using Von-Karman nonlinear relations and different plate theories, the time-dependent governing equations are obtained and then solved using the dynamic relaxation (DR) method combined with implicit Newmark's integration technique. Finally, some key elements namely: GPL weight fractions and distributions, porosity coefficients and dispersions, different loadings, boundary conditions, and the effects of thickness-to-radius ratio are discussed in detail. The results show that with an increase in porosity, the difference between the results of FSDT and MHSDT greatens. Also, a significant increase in plate stiffness is observed by adding a small amount of GPL to the porous core of the sandwich plate.

## 1. Introduction

The strength and stability of structures have always been two important principles in science that have attracted the attention of many scientists and researchers. For this purpose, for instance, in the construction of high-speed trains, space rockets, defense industries, and space shuttles they have tried to make materials as advanced and more resistant to various conditions. Due to their high tensile strength, sandwich structures have always been of great importance to manufacturers they are generally made of two or multi-layered composites usually with a central core fabricated of foams like polystyrene, honeycombs, balsa woods or other equivalent substances and two face sheets made of epoxies, glass, carbon, sheet metals or any other similar material.

Dynamic analysis of structures and plates with annular and circular geometries by various methods and theories has been carried out by many scientists and scholars because of their exclusive geometry and specific behavior under any sort of static and dynamic loadings and conditions. Working on determination of the dynamic response of large rectangular plates, Beskot and Leung [1] obtained the effects of viscoelastic damping values with the combination of FD, FE, and Laplace transform. Nath *et al.* [2] used the Chebyshev polynomial collocation point to couple with the Newmark k-β scheme for the time-dependent equations on plates and shells. Smaill [3] presented the importance of plate nonlinearity for the dynamic response of circular plates on Pasternak elastic foundations. Various numerical works are offered by Sirnivasan and Ramachandra [4] for different bore sizes on axisymmetric dynamic responses of annular and circular bimodulus plates. A study on the failure and dynamics of circular plates was done by Shen and Jones [5]. Day and Rao [6] studied the transient response of circular membranes and plates with the use of numerical Laplace transforms and finite difference in conjunction with numerical inversion technique, they presented the influence of interior and exterior viscoelastic damping on the responses. Bassi *et al.* [7] obtained pulsated results for sandwich plates using the FE method

* Corresponding author. Tel.: +985136625046; Fax: +985136629611
E-mail address: m.e.golmakani@mshdiau.ac.ir

and Galerkin's models. Submitting a new semi-analytical method for analyzing the vibrations of circular plates, Peng *et al*. [8] showed the accuracy of the proposed method among equivalent procedures. Damped schematics of a thick uniform plate under explosion loadings were analyzed including the rotary inertia influences by Aiyesimi *et al*. [9]. With the utilization of the FSDT of the Reddy plates, Eipakchi and Khadem Moshir [10] represented the viscoelastic resolutions for the transient response of annular plates. These are just a few of the limited and relevant aspects of the dynamic analysis of circular and annular plates with various material properties in the free literature done by individuals implementing various solving methods, showing the importance of such types of geometry in various engineering issues.

Failure and difficulties in achieving satisfying results have always been major obstacles for scientists, thus with the introduction of functionally graded materials, they have created a new direction of discovery to lead individuals in the field of engineering to facilitate and overcome the obstacles ahead. An FG structure consists of variations in compositional properties through the volume with specific functions of the material, frequently maintaining a ceramic matter embedded in a metallic matrix which will lead to the increase in thermal resistance, corrosion persistence, toughness in strength, and stiffness of the material. Moreover, even with the manufacturing of sandwich materials, one can consider another way of strengthening them for the tensile and compressive stresses. In this way, sandwich structures are usually considered from two-layer to multi-layer composites, and for example, in three-layer plates, the middle layer is considered from a type of foam or FG mode, and the outer plates are from one metal material. Using the sinusoidal shear deformation theory of plates, Zenkour [11] investigated the critical buckling and natural frequency of FGM sandwich plates. Subjecting FG circular plates under low-velocity impact loadings, Dai *et al*. [12] studied the significance of the primary velocity of a striking ball in the responses of the plate using the Newmark method. Three years later, Dai [13] investigated the transient response of an FG multi-layered circular plate with central disks to demonstrate the difference in geometry parameters of single-layer and sandwich plates. Dynamical bending of stepped variational width annular and circular functionally graded plates has been examined by Molla-Alipour [14] employing a semi-analytical method on the basis of power series. Effects of porosity on bending, buckling, free vibrations and dynamic instability behaviors of different FG plates and sandwich structures [15-21] are done by some researchers

on several geometries of beams, plates, and cylindrical shells with the application of various theories namely: FE, FD, DQM, Chebyshev-Ritz, HSDT, and isogeometric analysis. Babaei *et al*. [22], acquired natural frequencies and responses of FG annular sector plates and cylindrical shells with the acquisition of 3D elasticity theory. Implementing the kinetic dynamic relaxation method and FSDT formulations, Esmaeilzadeh *et al*. [23] developed a non-local strain gradient model for the numerical investigation of bilateral FG nanoplates with porous properties. Under pulse loadings, using a Kelvin-Voigt model, forced motions of viscoelastic FG porous beams are investigated by the use of the adopted FE method for the first time by Akbas *et al.* [24].

With further observations, porosity a well-noted item used in many works is one useful factor to overrule the flaws in mechanical properties of structures, despite their advantages such as ductility reductant, creep resistance, adhesion regressive and owning light weighting features, they contain a major defect which causes decreasing structural stiffness and strength. Thus, scientists and researchers have come to the conclusion of embedding certain structures with micro and nano fillers to overcome this deficiency. Free vibrations and buckling of graphene platelets (GPLs) reinforced FGM porous beams is the subject of an article surveyed by Kitipornchai *et al*. [25] based on the theory of Timoshenko beams and Ritz method for the natural fundamental frequency of the nanocomposite structure. On the same geometry with the same material properties, Chen *et al*. [26] studied the nonlinear responses and post-buckling behavior of GPL-reinforced material using the Von Karman nonlinear large deflections. Yang *et al*. [27], based on the Chebyshev-Ritz method and first-order shear deformation theory of plates, acted on the investigation of vibrations and buckling of porous nanocomposite plates reinforced by GPLs. Polit *et al*. [28] investigated the stability and bending results of porous GPL-reinforced curved beams based on the theory of higher-order shear deformation of plates by the introduction of Navier's procedure for the analytical results. Li *et al*. [29] studied the nonlinear responses and buckling solutions of a porous sandwich rectangular plate with Winkler-Pasternak foundations reinforced by graphene platelets for the observations of porosity effects and GPL weight fraction and loading velocity influence on the composite structure behavior. Esmaeilzadeh and Kadkhodayan [30] aimed the investigation of transient behaviors of a moving porous FGM sandwich rectangular nanoplate reinforced by GPLs and effects of non-local strain gradient parameters, porosity, GPL weight fraction, and

variant nanoplate velocities are considered in this paper. Safarpour *et al.* [31] considered a parametric 3D bending and frequency study on annular and circular functionally graded porous plates embedded with graphene nanofillers using DQM. Based on the theory of elasticity, Rahimi *et al.* [32], discussed on 3D static and vibrations of porous FG cylindrical shells in 2019. Zhao *et al.* [33], worked on instability factors affecting dynamic response of porous FG arches consolidated with GPL, based on Euler-Bernoulli classical theory. For the dynamic instable territory, a Galerkin approach was applied for the derivation of Mathieu-Hill equation. Their results show that by adding a small amount of GPL and with the use of uniform asymmetric distribution of porosities in arch composite plates, one can increase stability and resistance to a considerable extent. Lieu *et al.* [34] presented an isogeometric Bezier formulation for transient response and bending analysis of FG porous plates reinforced by GPL, deriving the equations of motions using a generalized HSDT in couple with Bezier isogeometric formulation and Newmark integration method for the time-varying equations. Based on modified strain gradient and first-order plates theory, Arshid *et al.* [35] studied on bending, buckling, and free vibrations of annular micro-scaled functionally graded porous plate which is reinforced with graphene nanoplatelets using the GDQ method. Results for wave propagation through FG-GPL reinforced porous rectangular plates were accomplished by Gao *et al.* [36] using three general plate theories namely CPT, FSDT, and TSDT. Results show that different plate theories can have accurate results on a lower number of waves, whilst the FSDT and TSDT show better results for a higher number of waves. Nejadi *et al.* [37] considered studies on vibrations and stability of sandwich pipes with porosities and GPLs using the differential quadrature method. In their paper, the essential impact of the velocity of fluid flow on the stability of the structure is illustrated. TAO and Dai [38] investigated the post-buckling of cylindrical sandwich porous shells with GPL reinforcement based on higher order shear deformation theory. Results show with more addition of GPL to the FG core, one can acquire much strength in post buckling behaviors. In 2020, Khayat *et al.* [39], analyzed uncertain dissemination over smart porous sandwich GPL reinforced cylindrical shells based on HSDT in conjunction with a Fourier differential quadrature method. Nguyen *et al.* [40-44] conducted several researches investigating the influence of porosity coefficient, weight fraction of GPLs, electrical voltage, material length scale parameter, boundary condition and dynamic loads on FG porous plates that are reinforced with GPLs. They proposed an efficient numerical model based on refined plate theory and isogeometric analysis to predict the static and dynamic characteristics of functionally graded microplates reinforced with graphene platelets. One disadvantage of the GPLs, that can be significantly challenging, is called the GPLs agglomeration phenomenon that can negatively impact the properties of the resulting nanocomposite material. The phenomenon occurs due to the strong van der Waals forces between the GPLs, which can lead to the formation of large aggregates. The presence of these aggregates can reduce the effective surface area and increase the stress concentrations in the nanocomposite, leading to a decrease in mechanical strength and an increase in brittleness. Nguyen *et al.* [45] studied the transient performance of agglomerated graphene platelets reinforced porous sandwich plates based on higher-order shear deformation plate theory and using a NURBS-based isogeometric analysis framework.

Through recent years, the combination of graphene nanofillers and porosity has been the focus of many researchers. Therefore, many works including bending, buckling, and post-buckling, free and forced vibrations are done and developed on various circular, rectangular, and shell geometries using various numerical solution and integration methods. With further observations and surveys through open literature, there was no evidence of dealing with nonlinear dynamics of FG annular porous plates reinforced with graphene platelets. This paper aims the study of dynamic analysis of annular functionally graded porous GPL-reinforced sandwich plates using FSDT and MHSDT with two GPL distribution patterns and two porosity dispersions, under a simple harmonic and an impact loading with clamped and simply supported boundary conditions. GPLs reinforcement phase in this work is distributed through the core of the sandwich plate. In sandwich plate structures, the distribution of the GPLs reinforcement phase in the core layer can enhance mechanical properties, such as compressive and shear strength [29]. Moreover, distributing GPLs in the core layer can create a highly interconnected network within the core material and the mechanical properties and resistance to fatigue and impact of the sandwich structure can be improved [30]. The time-dependent equations are derived by the implementation of the principle of minimum potential energy and then solved using Newmark's direct integration method in combination with the viscous dynamic relaxation technique, which has not been previously employed in the literature for analyzing the dynamic behavior of sandwich structures.

Finally, the effects of porosity coefficient and dispersions, GPL weight fraction and dispensations and thickness-to-radius ratios are illustrated.

## 2. Theoretical Modeling of Material Properties

As seen in Fig. 1, the annular FG sandwich graphene-reinforced porous plate is shown with an inner radius $r_i$ and outer radius $r_o$, the total thickness of $h$ (including $h_c$= core and $h_f$= face layers thicknesses) in $r$ and $z$ directions, originated the Cartesian coordinate is assumed at the center of the plate. The whole thickness of the plate includes $h_c + 2h_f$.
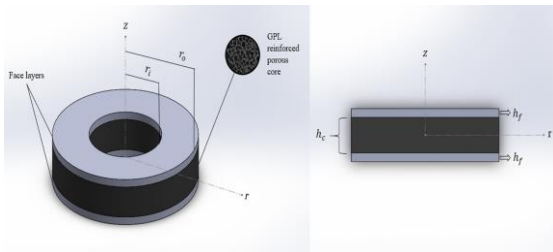


**Fig. 1.** Geometrical illustration of annular graphene-reinforced porous sandwich plate

Figure 2 represents two GPL distributions, namely A and B with different porosity dispersion patterns as I and II for symmetric and asymmetric material. The volume fraction of the GPL as $V_{gpl}$ is assumed to be varying along the $z$ axis, with maximum values of $S_{ii}$ and $S_{ij}$ (see relation (7)).

According to Fig. 2, E(z), G(z), and ρ(z) which are named elasticity moduli, shear moduli, and mass density of the porous GPL-reinforced sandwich plate, respectively, are defined as below for non-uniform graphene distributions [46]:

$$E(z) = E^*(1 - e_0\phi(z)),$$
$$G(z) = \frac{E(z)}{2(1 + v(z))}, \tag{1}$$
$$\rho(z) = \rho^*(1 - e_m\phi(z)).$$

in which $\phi(z)$ is defined as [47]:

$$\phi(z) = cos\left(\frac{\pi z}{2h_c} + \frac{\pi}{4}\right),$$

*For asymmetric porosity dispersion*

$$\phi(z) = cos\left(\frac{\pi z}{h_c}\right). \tag{2}$$

*For symmetric porosity dispersion*

Also, $e_0$ denotes porosity coefficient $(0 < e_0 < 1)$ and $e_m$ is the representative of the mass density coefficient. On the basis of the closed-cell cellular solid structures under the Gaussian Random Field scheme (GRF), it can be expressed to determine the mass density coefficient as [48]:

$$e_m = \frac{1.121(1 - \sqrt[2.3]{1 - e_0\phi(z)})}{\phi(z)}. \tag{3}$$

Furthermore, based on the micromechanical model of Halpin-Tsai, the effective elastic moduli of the porous core can be defined as [49]:

$$E^* = \frac{3}{8}\left(\frac{1 + \varsigma_l^{gpl}\iota_l^{gpl}V_{gpl}}{1 - \iota_l^{gpl}V_{gpl}}\right)E_m$$
$$+ \frac{5}{8}\left(\frac{1 + \varsigma_w^{gpl}\iota_w^{gpl}V_{gpl}}{1 - \iota_w^{gpl}V_{gpl}}\right)E_m. \tag{4}$$

where $\varsigma^{gpl}$ and $\iota^{gpl}$ are the GPL property factors, also $E_m$ depict the young's moduli of the metallic matrix. For the unknown values of the GPL factors, we have [49]:
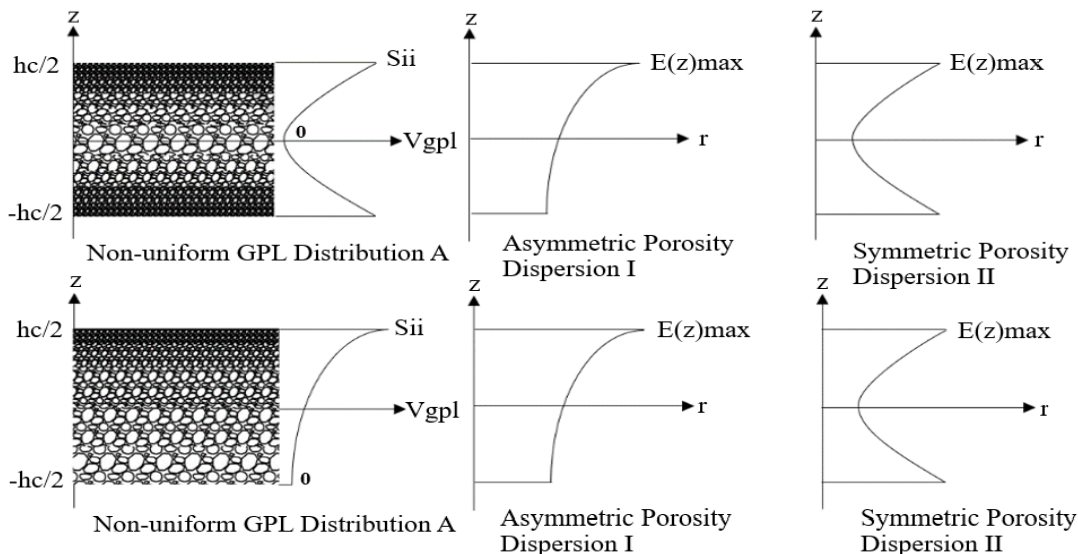


**Fig. 2.** GPL distributions and porosity dispersion patterns

$$\varsigma_l^{gpl} = \frac{2l_{gpl}}{t_{gpl}},$$

$$\varsigma_w^{gpl} = \frac{2w_{gpl}}{t_{gpl}},$$

$$\iota_l^{gpl} = \frac{\left(E_{gpl}/E_m\right) - 1}{\left(E_{gpl}/E_m\right) + \varsigma_l^{gpl}},$$

$$\iota_w^{gpl} = \frac{\left(E_{gpl}/E_m\right) - 1}{\left(E_{gpl}/E_m\right) + \varsigma_w^{gpl}}. \tag{5}$$

where $l_{gpl}$, $w_{gpl}$ and $t_{gpl}$ are the average length, width, and thickness of the GPLs, respectively. Also, based on the GRF scheme, the varying Poisson's ratio of the core is obtained by [50]:

$$\begin{aligned}\nu(z) = {}& 0.221\phi(z)e_m \\ & + \nu^*(0.342(\phi(z)e_m)^2 - 1.21\phi(z)e_m + 1)\end{aligned} \tag{6}$$

As depicted in Fig. 2, for different GPL distribution patterns, the volume fraction distribution ($V_{gpl}$) along the z direction is given by [51]:

$$V_{gpl} = \begin{cases} s_{ii}\left[1 - cos(\frac{\pi z}{h_c})\right], & \text{GPL distribution A} \\ s_{ij}\left[1 - cos(\frac{\pi z}{2h_c} + \frac{\pi}{4})\right]. & \text{GPL distribution B} \end{cases} \tag{7}$$

in which the relationship between the volume fraction and weight fraction of the GPLs is defined by [52]:

$$\begin{aligned} & \frac{W_{gpl}}{W_{gpl} + \frac{\rho_{gpl}}{\rho_m} - \frac{\rho_{gpl}}{\rho_m}W_{gpl}} \\ & \quad \times \int_{\frac{-h_c}{2}}^{\frac{h_c}{2}} [1 - e_m\phi(z)]dz \\ & = \int_{\frac{-h_c}{2}}^{\frac{h_c}{2}} V_{gpl}[1 - e_m\phi(z)]dz \end{aligned} \tag{8}$$

Utilizing the rule of mixture, $\rho^*$ and $\nu^*$ the mass density and Poisson's ratio of the GPL-reinforced platelets, respectively, can be calculated as below [53]:

$$\rho^* = \rho_{gpl}V_{gpl} + \rho_m V_m,$$

$$\nu^* = \nu_{gpl}V_{gpl} + \nu_m V_m,$$

$$V_m = 1 - V_{gpl}. \tag{9}$$

in which $\rho_{gpl}$, $\nu_{gpl}$, $V_{gpl}$, $\rho_m$, $\nu_m$ and $V_m$ are mass density, Poisson's ratio, and volume fraction of GPLs and metals, respectively.
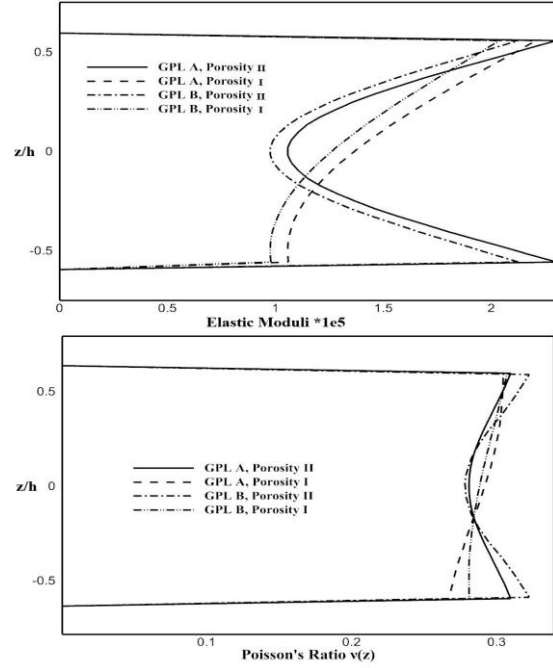


**Fig. 3**. Modules of elasticity and Poisson's ratio along the thickness of the sandwich plate for different GPLs distributions and porosity patterns

Modules of elasticity and Poisson's ratio of the sandwich plate are illustrated in Fig. 3 for different GPLs distributions and porosity patterns using the properties expressed in Table 3.

## 3. Fundamental Equations

Based on the modified higher-order shear deformation theory (primarily proposed by [54]), the displacement field of the plate is described by:

*MHSDT =*

$$\begin{cases} U(r, z, t) = u(r, t) + z\varphi_r(r, t) + f(z)\psi_r(r, t), \\ V(r, z, t) = 0, \\ W(r, z, t) = w(r, t). \end{cases} \tag{10}$$

where the displacements of the composite plate are formed of $U$, $V$, and $W$ in the orthogonal coordinate system. Moreover, $u$ and $w$ are the displacements along r and z axes and also $\varphi_r$ is the rotation terms of the middle surface (i.e., z = 0). Furthermore, the term $\psi_r$ in MHSDT is a mathematical parameter that cannot be physically defined.

Besides, *f(z)* is a functional term that can be presumed as required in calculation. It should be noted that considering *f(z)* as 0, one can consider the first-order shear deformation theory of the plates (FSDT) for the displacement field.

The simplicity and efficiency of using this theory are considering various functions in the displacement field and obtaining accurate results for different conditions.

Considering the Von-Karman nonlinear large deflection relation, the strain field accommodating with the displacement field of equation (10) is defined as follows:

$$
\begin{Bmatrix} \varepsilon_r \\ \varepsilon_\theta \\ \gamma_{rz} \end{Bmatrix} =
$$

$$
\begin{Bmatrix} \frac{\partial u}{\partial r} + \frac{1}{2}\left(\frac{\partial w}{\partial r}\right)^2 + z\frac{\partial \varphi_r}{\partial r} + f(z)\frac{\partial \psi_r}{\partial r} \\[2mm] \frac{u}{r} + z\frac{\varphi_r}{r} + \frac{f(z)}{r}\psi_r \\[2mm] \frac{\partial w}{\partial r} + \varphi_r + f'(z)\psi \end{Bmatrix},
$$

$$
\frac{-h_c}{2} - hf < z < \frac{h_c}{2} + hf. \tag{11}
$$

in which normal strain fields $\varepsilon_r$ and $\varepsilon_\theta$ are directed towards $r$ and $\theta$, respectively, and $\gamma_{rz}$ is the shear strain term. According to Hook's law, the stress field for the core and face layers, are:

$$
\begin{bmatrix} \sigma_r \\ \sigma_\theta \\ \sigma_{rz} \end{bmatrix} =
$$

$$
\begin{bmatrix} Q_{11} = \frac{E_f}{1-\nu_f^2} & Q_{12} = \frac{\nu_f E_f}{1-\nu_f^2} & 0 \\[2mm] Q_{21} = \frac{\nu_f E_f}{1-\nu_f^2} & Q_{22} = \frac{E_f}{1-\nu_f^2} & 0 \\[2mm] 0 & 0 & Q_{66} = G_f = \frac{E_f}{2(1+\nu_f)} \end{bmatrix} \begin{bmatrix} \varepsilon_r \\ \varepsilon_\theta \\ \gamma_{rz} \end{bmatrix}
$$

*For Face layers* (12)

$$
\begin{bmatrix} \sigma_r \\ \sigma_\theta \\ \sigma_{rz} \end{bmatrix} =
$$

$$
\begin{bmatrix} Q_{11} = \frac{E(z)}{1-\nu(z)^2} & Q_{12} = \frac{\nu(z)E(z)}{1-\nu(z)^2} & 0 \\[2mm] Q_{21} = \frac{\nu(z)E(z)}{1-\nu(z)^2} & Q_{22} = \frac{E(z)}{1-\nu(z)^2} & 0 \\[2mm] 0 & 0 & Q_{66} = G(z) = \frac{E(z)}{2(1+\nu(z))} \end{bmatrix} \begin{bmatrix} \varepsilon_r \\ \varepsilon_\theta \\ \gamma_{rz} \end{bmatrix}
$$

*For GPL porous core* (13)

Stress and moment resultants are defined as:

$$
(N_i, M_i, R_i) =
$$

$$
\left\{ \int_{h_c/2}^{h_f + h_c/2} \left(1, z, f(z)\right)\sigma_i dz + \right.
$$

$$
\int_{-h_c/2}^{h_c/2} \left(1, z, f(z)\right)\sigma_i dz +
$$

$$
\left. \int_{-h_c/2 - h_f}^{-h_c/2} \left(1, z, f(z)\right)\sigma_i dz \right\}, \quad i = r, \theta, \tag{14}
$$

$$
(Q_{rz}, R_{rz})
$$

$$
= \left\{ \int_{h_c/2}^{h_f + h_c/2} (\sigma_{rz}, f'(z)\sigma_{rz}) dz \right.
$$

$$
+ \int_{-h_c/2}^{h_c/2} (\sigma_{rz}, f'(z)\sigma_{rz}) dz
$$

$$
\left. + \int_{-h_c/2 - h_f}^{-h_c/2} (\sigma_{rz}, f'(z)\sigma_{rz}) dz \right\}. \tag{15}
$$

Substituting equations $(11-13)$ into $(14-15)$ leads to the following constitutive relations:

$$
N_r = A\left\{\frac{\partial u}{\partial r} + \frac{1}{2}\left(\frac{\partial w}{\partial r}\right)^2 + \nu\frac{u}{r}\right\} +
$$

$$
B\left\{\frac{\partial \varphi_r}{\partial r} + \nu\frac{\varphi_r}{r}\right\} + C\left\{\frac{\partial \psi_r}{\partial r} + \nu\frac{\psi_r}{r}\right\}, \tag{16}
$$

$$
N_\theta = A\left\{\nu\frac{\partial u}{\partial r} + \frac{\nu}{2}\left(\frac{\partial w}{\partial r}\right)^2 + \frac{u}{r}\right\} +
$$

$$
B\left\{\nu\frac{\partial \varphi_r}{\partial r} + \frac{\varphi_r}{r}\right\} + C\left\{\nu\frac{\partial \psi_r}{\partial r} + \frac{\psi_r}{r}\right\}, \tag{17}
$$

$$
M_r = B\left\{\frac{\partial u}{\partial r} + \frac{1}{2}\left(\frac{\partial w}{\partial r}\right)^2 + \nu\frac{u}{r}\right\} +
$$

$$
F\left\{\frac{\partial \varphi_r}{\partial r} + \nu\frac{\varphi_r}{r}\right\} + G\left\{\frac{\partial \psi_r}{\partial r} + \nu\frac{\psi_r}{r}\right\}, \tag{18}
$$

$$
M_\theta = B\left\{\nu\frac{\partial u}{\partial r} + \frac{\nu}{2}\left(\frac{\partial w}{\partial r}\right)^2 + \frac{u}{r}\right\} +
$$

$$
F\left\{\nu\frac{\partial \varphi_r}{\partial r} + \frac{\varphi_r}{r}\right\} + G\left\{\nu\frac{\partial \psi_r}{\partial r} + \frac{\psi_r}{r}\right\}, \tag{19}
$$

$$
R_r = C\left\{\frac{\partial u}{\partial r} + \frac{1}{2}\left(\frac{\partial w}{\partial r}\right)^2 + \nu\frac{u}{r}\right\} +
$$

$$
G\left\{\frac{\partial \varphi_r}{\partial r} + \nu\frac{\varphi_r}{r}\right\} + H\left\{\frac{\partial \psi_r}{\partial r} + \nu\frac{\psi_r}{r}\right\}, \tag{20}
$$

$$
R_\theta = C\left\{\nu\frac{\partial u}{\partial r} + \frac{\nu}{2}\left(\frac{\partial w}{\partial r}\right)^2 + \frac{u}{r}\right\} +
$$

$$
G\left\{\nu\frac{\partial \varphi_r}{\partial r} + \frac{\varphi_r}{r}\right\} + H\left\{\nu\frac{\partial \psi_r}{\partial r} + \frac{\psi_r}{r}\right\}, \tag{21}
$$

$$
Q_{rz} = D\left\{\varphi + \frac{\partial w}{\partial r}\right\} + E\{\psi\}, \tag{22}
$$

$$
R_{rz} = E\left\{\varphi + \frac{\partial w}{\partial r}\right\} + I\{\psi\}. \tag{23}
$$

Where the elastic constants are expressed as:

$$
(A_{ij}, B_{ij}, C_{ij}, F_{ij}, G_{ij}, H_{ij}) =
$$

$$
\left( \int_{h_c/2}^{h_f + h_c/2} Q_{ij\,f}^{(1)} \left(1, z, f(z), z^2, zf(z), f^2(z)\right) dz + \right.
$$

$$
\int_{-h_c/2}^{h_c/2} Q_{ij\,c}^{(2)} \left(1, z, f(z), z^2, zf(z), f^2(z)\right) dz +
$$

$$
\left. \int_{-h_c/2 - h_f}^{-h_c/2} Q_{ij\,f}^{(3)} \left(1, z, 1, z, f(z), z^2, zf(z), f^2(z)\right) dz \right.
$$

$$
ij = 11, 12, 22 \tag{24}
$$

$$
(D, E, I) =
$$

$$
\left( \int_{h_c/2}^{h_f + h_c/2} Q_{66\,f}^{(1)}(1, f'(z), f'(z)^2) \, dz + \right.
$$

$$
\int_{-h_c/2}^{h_c/2} Q_{66\,c}^{(2)}(1, f'(z), f'(z)^2) \, dz +
$$

$$
\left. \int_{-h_c/2 - h_f}^{-h_c/2} Q_{66\,f}^{(3)}(1, f'(z), f'(z)^2) \, dz \right). \tag{25}
$$

in which $Q^{(n)}$ expresses the stiffness matrix of the layer number ($n$) as follows:

$$
Q^{(n)} = \begin{bmatrix} Q_{11} & Q_{12} & 0 \\ Q_{12} & Q_{22} & 0 \\ 0 & 0 & Q_{66} \end{bmatrix}^n. \tag{26}
$$

The equations of motion can be obtained by implementation of the principle of minimum

potential energy, which is expressed by the following integral:

$$\delta\Pi = \int_0^\tau (\delta U + \delta W - \delta K)\,dt = 0. \qquad (27)$$

in which $\delta U$, $\delta W$, and $\delta K$ are strain energy changes due to internal loads, work changes due to external loads, and virtual kinetic energy changes, respectively.

Changes in strain energy, virtual work, and kinetic energy of the whole system are defined as:

$$\begin{cases} \delta U = \int_0^\tau \int_V (\sigma_r \delta\varepsilon_r + \sigma_\theta \delta\varepsilon_\theta + \sigma_{rz}\delta\gamma_{rz})\,dV dt, \\[2mm] \delta W = \int_0^\tau \int_{r_i}^{r_o} \int_0^{2\pi} (F(t))\,\delta w\, r dr d\theta dt, \\[2mm] \delta K = \frac{1}{2}\int_0^\tau \int_V \rho\delta\left[\left(\frac{\partial u}{\partial t}\right)^2 + \left(\frac{\partial w}{\partial t}\right)^2\right]dV dt. \end{cases} \qquad (28)$$

For instance, by substituting strain components in terms of displacement field into the variations in strain energy relation yields:

$$\delta U = \iiint_V \left(\sigma_r \delta\left(\frac{\partial u}{\partial r} + \frac{1}{2}\left(\frac{\partial w}{\partial r}\right)^2 + z\frac{\partial\varphi_r}{\partial r} + f(z)\frac{\partial\psi_r}{\partial r}\right) + \sigma_\theta \delta\left(\frac{u}{r} + z\frac{\varphi_r}{r} + \frac{f(z)}{r}\psi\right) + \sigma_{rz}\delta\left(\frac{\partial w}{\partial r} + \varphi_r + f'(z)\right)\right)r dr d\theta dz. \qquad (29)$$

By integrating over the thickness of Eq. (29) and substituting the stress and moment results, the following equation for the total thickness of the plate will be obtained:

$$\delta U = \iint_A \left(\left(N_r\delta\frac{\partial u}{\partial r} + N_r\frac{\partial w}{\partial r}\delta\frac{\partial w}{\partial r} + M_r\delta\frac{\partial\varphi_r}{\partial r} + R_r\delta\frac{\partial\psi_r}{\partial r}\right) + \left(N_\theta\delta\frac{u}{r} + M_\theta\delta\frac{\varphi_r}{r} + R_\theta\delta\frac{\psi_r}{r}\right) + \left(Q_{rz}\delta\frac{\partial w}{\partial r} + Q_{rz}\delta\varphi_r + R_{rz}\delta\psi_r\right)\right)r dr d\theta. \qquad (30)$$

Integrating from each term of relation (30) and implementing the fractional integration technique, results in the below relation in which the singleton integrals show the boundary conditions and the dual integrals represent the governing equations:

$$\delta U$$

$$= -\iint_A \left\{ \begin{array}{l} \left[N_r + r\frac{\partial N_r}{\partial r} - N_\theta\right]\delta u + \\[2mm] \left[r\frac{\partial M_r}{\partial r} + M_r - M_\theta - rQ_{rz}\right]\delta\varphi_r + \\[2mm] \left[r\frac{\partial R_r}{\partial r} + R_r - R_\theta - rR_{rz}\right]\delta\psi_r + \\[2mm] \left[\frac{\partial}{\partial r}\left(rN_r\frac{\partial w}{\partial r} + r\frac{\partial Q_{rz}}{\partial r} + Q_{rz}\right)\right]\delta w \end{array} \right\} dr d\theta$$

$$+ \oint_\Gamma \left\{ \begin{array}{c} [rN_r d\theta]\delta u + [rM_r d\theta]\delta\varphi_r \\ + [rR_r d\theta]\delta\psi_r \\ + \left[rN_r\frac{\partial w}{\partial r} + rQ_{rz}\right]\delta w \end{array} \right\} d\Gamma \qquad (31)$$

By introducing mass inertia terms as follows:

$$I_j =$$

$$\int_{h_c/2}^{h_f + h_c/2} \rho_f(1, z, z^2, f(z), (z.f(z)), (f(z))^2)\,dz$$

$$\int_{-h_c/2}^{h_c/2} \rho(z)(1, z, z^2, f(z), (z.f(z)), (f(z))^2)\,dz$$

$$\int_{-h_c/2 - h_f}^{-h_c/2} \rho_f(1, z, z^2, f(z), (z.f(z)), (f(z))^2)\,dz$$

$$j = 1, 2, 3, 4, 5, 6 \qquad (32)$$

The kinetic energy changes can be expressed by:

$$\int_0^T \delta K dt = \int_T \left\{ \iint_A \left[I_1\dot U\delta\dot U - I_2\dot U\delta\dot\varphi_r - I_4\dot U\delta\dot\psi_r + I_2\dot\varphi_r\delta\dot U + I_3\dot\varphi_r\delta\dot\varphi_r + I_5\dot\varphi_r\delta\dot\psi_r - I_4\dot\psi_r\delta\dot U + I_5\dot\psi_r\delta\dot\varphi_r + I_6\dot\varphi_r\delta\dot\varphi_r + I_1\dot W\delta\dot W\right]dA \right\}dt. \qquad (33)$$

Finally, substituting Eq. (28) into Eq. (27) and giving zero to $\delta u$, $\delta\varphi_r$, $\delta\psi_r$ and $\delta w$, the equations of motion will result in [55]:

$$\frac{\partial N_r}{\partial r} + \left(\frac{N_r - N_\theta}{r}\right) = \left(I_1\frac{\partial^2 u}{\partial t^2} + I_2\frac{\partial^2\varphi_r}{\partial t^2} + I_4\frac{\partial^2\psi_r}{\partial t^2}\right),$$

$$\frac{\partial M_r}{\partial r} - Q_{rz} + \left(\frac{M_r - M_\theta}{r}\right) = \left(I_2\frac{\partial^2 u}{\partial t^2} + I_3\frac{\partial^2\varphi_r}{\partial t^2} + I_5\frac{\partial^2\psi_r}{\partial t^2}\right),$$

$$\frac{\partial R_r}{\partial r} - R_{rz} + \left(\frac{R_r - R_\theta}{r}\right) = \left(I_4\frac{\partial^2 u}{\partial t^2} + I_3\frac{\partial^2\varphi_r}{\partial t^2} + I_6\frac{\partial^2\psi_r}{\partial t^2}\right),$$

$$\frac{\partial Q_{rz}}{\partial r} + \frac{Q_{rz}}{r} + \left(N_r\frac{\partial^2 w}{\partial r^2} + \frac{N_\theta}{r}\frac{\partial w}{\partial r}\right) + F(t) = \left(I_1\frac{\partial^2 w}{\partial t^2}\right). \qquad (34)$$

We could also obtain the static equilibrium equations in terms of displacement field $u$, $w$, $\varphi_r$ and $\psi_r$ as follows:

$$A_{11}\left(\frac{\partial^2 u}{\partial r^2} + \left(\frac{1}{2}\right)\frac{\partial}{\partial r}\left(\frac{\partial w}{\partial r}\right)^2\right) +$$

$$A_{12}\left(\frac{\partial}{\partial r}\left(\frac{u}{r}\right)\right) + B_{11}\frac{\partial^2 \varphi_r}{\partial r^2} +$$

$$B_{12}\left(\frac{\partial}{\partial r}\left(\frac{\varphi_r}{r}\right)\right) + C_{11}\left(\frac{\partial^2 \psi_r}{\partial r^2}\right) +$$

$$C_{12}\left(\frac{\partial}{\partial r}\left(\frac{\psi_r}{r}\right)\right) + \frac{1}{r}\left\{\left(\frac{\partial u}{\partial r} + \right.\right.$$

$$\left(\frac{1}{2}\right)\left(\frac{\partial w}{\partial r}\right)^2\right)(A_{11} - A_{12}) + \frac{u}{r}(A_{12} -$$

$$A_{22}) + \frac{\partial \varphi_r}{\partial r}(B_{11} - B_{12}) + \frac{\varphi_r}{r}(B_{12} -$$

$$B_{22}) + \frac{\partial \psi_r}{\partial r}(C_{11} - C_{12}) + \frac{\psi_r}{r}(C_{12} -$$

$$C_{22})\Big\} = 0, \tag{35}$$

$$B_{11}\left(\frac{\partial^2 u}{\partial r^2} + \left(\frac{1}{2}\right)\frac{\partial}{\partial r}\left(\frac{\partial w}{\partial r}\right)^2\right) +$$

$$B_{12}\left(\frac{\partial}{\partial r}\left(\frac{u}{r}\right)\right) + F_{11}\frac{\partial^2 \varphi_r}{\partial r^2} +$$

$$F_{12}\left(\frac{\partial}{\partial r}\left(\frac{\varphi_r}{r}\right)\right) + G_{11}\left(\frac{\partial^2 \psi_r}{\partial r^2}\right) +$$

$$G_{12}\left(\frac{\partial}{\partial r}\left(\frac{\psi_r}{r}\right)\right) + \frac{1}{r}\left\{\left(\frac{\partial u}{\partial r} + \right.\right.$$

$$\left(\frac{1}{2}\right)\left(\frac{\partial w}{\partial r}\right)^2\right)(B_{11} - B_{12}) + \frac{u}{r}(B_{12} -$$

$$B_{22}) + \frac{\partial \varphi_r}{\partial r}(F_{11} - F_{12}) + \frac{\varphi_r}{r}(F_{12} -$$

$$F_{22}) + \frac{\partial \psi_r}{\partial r}(G_{11} - G_{12}) + \frac{\psi_r}{r}(G_{12} -$$

$$G_{22})\Big\} - D\left(\varphi_r + \frac{\partial w}{\partial r}\right) - E(\psi) = 0, \tag{36}$$

$$C_{11}\left(\frac{\partial^2 u}{\partial r^2} + \left(\frac{1}{2}\right)\frac{\partial}{\partial r}\left(\frac{\partial w}{\partial r}\right)^2\right) +$$

$$C_{12}\left(\frac{\partial}{\partial r}\left(\frac{u}{r}\right)\right) + G_{11}\frac{\partial^2 \varphi_r}{\partial r^2} +$$

$$G_{12}\left(\frac{\partial}{\partial r}\left(\frac{\varphi_r}{r}\right)\right) + H_{11}\left(\frac{\partial^2 \psi_r}{\partial r^2}\right) +$$

$$H_{12}\left(\frac{\partial}{\partial r}\left(\frac{\psi_r}{r}\right)\right) + \frac{1}{r}\left\{\left(\frac{\partial u}{\partial r} + \right.\right.$$

$$\left(\frac{1}{2}\right)\left(\frac{\partial w}{\partial r}\right)^2\right)(C_{11} - C_{12}) + \frac{u}{r}(C_{12} -$$

$$C_{22}) + \frac{\partial \varphi_r}{\partial r}(G_{11} - G_{12}) + \frac{\varphi_r}{r}(G_{12} -$$

$$G_{22}) + \frac{\partial \psi_r}{\partial r}(H_{11} - H_{12}) + \frac{\psi_r}{r}(H_{12} -$$

$$H_{22})\Big\} - e\left(\varphi_r + \frac{\partial w}{\partial r}\right) - I(\psi) = 0, \tag{37}$$

$$\left\{\left[A_{11}\left(\frac{\partial u}{\partial r} + \left(\frac{1}{2}\right)\left(\frac{\partial w}{\partial r}\right)^2\right)\right]\frac{\partial^2 w}{\partial r^2}\right\} +$$

$$A_{12}\left(\frac{u}{r}\right) + B_{11}\left(\frac{\partial \varphi_r}{\partial r}\right) + B_{12}\left(\frac{\varphi_r}{r}\right) +$$

$$C_{11}\left(\frac{\partial \psi_r}{\partial r}\right) + C_{12}\left(\frac{\psi_r}{r}\right) + \left\{\left[A_{12}\left(\frac{\partial u}{\partial r} + \right.\right.\right.$$

$$\left(\frac{1}{2}\right)\left(\frac{\partial w}{\partial r}\right)^2\right)\Big]\frac{1}{r}\frac{\partial w}{\partial r} + A_{22}\left(\frac{u}{r}\right) +$$

$$B_{12}\left(\frac{\partial \varphi_r}{\partial r}\right) + B_{22}\left(\frac{\varphi_r}{r}\right) + C_{12}\left(\frac{\partial \psi_r}{\partial r}\right) +$$

$$C_{22}\left(\frac{\psi_r}{r}\right) + D\left(\frac{\partial \varphi_r}{\partial r} + \frac{\partial^2 w}{\partial r^2}\right) + D\left(\frac{\varphi_r}{r} + \right.$$

$$\left.\frac{\partial w}{r\partial r}\right) + E\left(\frac{\partial \psi_r}{\partial r} + \frac{\psi_r}{r}\right) = 0. \tag{38}$$

To complete the formulations, equations $(35 - 38)$ should be joined with a set of initial and boundary conditions, as below:

$$\text{Initial conditions at } t = 0: \begin{cases} u = 0 \\ \varphi = 0 \\ \psi = 0 \\ w = 0 \end{cases}$$

$$\text{Boundary conditions:} \begin{cases} \text{Clamped supported at } r_i, r_o: \begin{cases} u = 0 \\ \varphi = 0 \\ \psi = 0 \\ w = 0 \end{cases} \\ \text{Simply supported at } r_i, r_o: \begin{cases} u = 0 \\ w = 0 \\ M_r = 0 \\ R_r = 0 \end{cases} \end{cases}$$

## 4. Solving Procedure

To discretize the time-dependent equations of motion of annular GPL-reinforced porous sandwich composite plate, the implicit Newmark method is utilized in this paper, and in order to solve the partial differential equations of motion, the viscous dynamic relaxation method (V-DR) with central finite difference technique is exploited.

### 4.1. Newmark Direct Integration Method

The main aim of the Newmark approach is to discretize the time-varying equations using a reduced Taylor series by determination of accelerations and velocities in real forms at the next time step $(t_{j+1})$ as:

$$\ddot{\chi}_{j+1} = \left\{(\chi_{j+1} - \chi_j)\frac{1}{\beta(\Delta t_j)^2} - \right.$$

$$\dot{\chi}_j\left(\frac{1}{\beta \Delta t_j}\right) - \ddot{\chi}_j\left(\frac{1}{2\beta} - 1\right)\right\}, \tag{40}$$

$$\dot{\chi}_{j+1} = \left\{(\chi_{j+1} - \chi_j)\frac{\gamma}{\beta \Delta t_j} - \dot{\chi}_j\left(\frac{\gamma}{\beta} - 1\right) - \right.$$

$$\ddot{\chi}_j\Delta t_j\left(\frac{\gamma}{2\beta} - 1\right)\right\}. \tag{41}$$

where $\gamma$ and $\beta$ are Newmark's constant parameters which can be determined to gain integration stability and accuracy, taken as 0.5 and 0.25 (average acceleration method), $\Delta t$ is the time interval, the difference of current and prior real-time displacement, velocity, and acceleration, respectively. Also, $\chi$ represents the displacements ($\chi = u, \varphi, \psi, w$) at $t_{j+1}$ and $t_j$. Placing equations (40) and (41) into (34) the equilibrium equations will become:

$$\frac{\partial N_r}{\partial r} + \left(\frac{N_r - N_\theta}{r}\right)$$

$$-A_1\left(I_1 u_{j+1} + I_2 \varphi_{r_{j+1}} + I_4 \psi_{r_{j+1}}\right) =$$

$$I_1\left(A_1 u_j + A_2 \dot{u}_j + A_3 \ddot{u}_j\right)$$

$$-\langle +I_2\left(A_1 \varphi_{r_j} + A_2 \dot{\varphi}_{r_j} + A_3 \ddot{\varphi}_{r_j}\right)\rangle,$$

$$+I_4\left(A_1 \psi_{r_j} + A_2 \dot{\psi}_{r_j} + A_3 \ddot{\psi}_{r_j}\right) \tag{42}$$

$$\frac{\partial M_r}{\partial r} - Q_{rz} + \left(\frac{M_r - M_\theta}{r}\right)$$
$$- A_1 \big(I_2 u_{j+1}$$
$$+ I_3 \varphi_{r_{j+1}} + I_5 \psi_{r_{j+1}}\big)$$
$$=$$
$$I_2\big(A_1 u_j + A_2 \dot{u}_j + A_3 \ddot{u}_j\big)$$
$$- \langle + I_3\big(A_1 \varphi_{r_j} + A_2 \dot{\varphi}_{r_j} + A_3 \ddot{\varphi}_{r_j}\big)\rangle,$$
$$+ I_5\big(A_1 \psi_{r_j} + A_2 \dot{\psi}_{r_j} + A_3 \ddot{\psi}_{r_j}\big) \qquad (43)$$

$$\frac{\partial R_r}{\partial r} - R_{rz} + \left(\frac{R_r - R_\theta}{r}\right)$$
$$- A_1 \big(I_4 u_{j+1}$$
$$+ I_3 \varphi_{r_{j+1}} + I_6 \psi_{r_{j+1}}\big)$$
$$=$$
$$I_4\big(A_1 u_j + A_2 \dot{u}_j + A_3 \ddot{u}_j\big)$$
$$- \langle + I_3\big(A_1 \varphi_{r_j} + A_2 \dot{\varphi}_{r_j} + A_3 \ddot{\varphi}_{r_j}\big)\rangle,$$
$$+ I_6\big(A_1 \psi_{r_j} + A_2 \dot{\psi}_{r_j} + A_3 \ddot{\psi}_{r_j}\big) \qquad (44)$$

$$\frac{\partial Q_{rz}}{\partial r} + \frac{Q_{rz}}{r} + \left(N_r \frac{\partial^2 w}{\partial r^2} + \frac{N_\theta}{r}\frac{\partial w}{\partial r}\right)$$
$$- A_1\big(I_1 w_{j+1}\big) =$$
$$-I_1\big(A_1 w_j + A_2 \dot{w}_j + A_3 \ddot{w}_j\big) - F(t). \qquad (45)$$

where the following are Newmark coefficients:

$$A_1 = \frac{1}{\beta(\Delta t_j)^2}, \; A_2 = \frac{1}{\beta \Delta t_j}, \; A_2 = \frac{1}{2\beta} - 1. \qquad (46)$$

Hence, for the sake of briefness, the following shrunken term should be written for the equations of motion:

$$\big[K_{j+1}\big]^n \{\chi_{j+1}\}^n = \{P(t_{j+1})\}^n. \qquad (47)$$

in which $\{P(t_{j+1})\}^n$ and $\big[K_{j+1}\big]^n$ are the equivalent load vector and stiffness matrix at $n^{th}$ DR iteration.

### 4.2. Viscous Damping Dynamic Relaxation Method

Based on the dynamic relaxation method, to obtain stable solutions, the governing equations of motion (47) will be converted from a static space into a fictitious dynamic one via the transformation of boundary value into initial value problems. The conversion would happen through the addition of damping and inertia terms to equilibrium equations [56]:

$$[M]\{\ddot{\chi}\}^n + [C]\{\dot{\chi}\}^n + \big[K_{j+1}\big]^n \{\chi_{j+1}\}^n$$
$$= \{P(t_{j+1})\}^n. \qquad (48)$$

in which $[M]$ and $[C]$ in the above relation are fictitious diametrical mass and damping matrices respectively, also $\{\ddot{\chi}\}^n$ and $\{\dot{\chi}\}^n$ are the acceleration and velocity, respectively. Accurate estimations of mass matrix and damping factors are the criteria of convergence and stability in the DR method, thus based on the theorem of Gershgorin, they will be estimated as [56]:

$$m_{ii}^d \geq \frac{1}{4}[\tau^n]^2 \sum_{l=1}^{N}|k_{il}|, \qquad (49)$$

$$c_i^n = 2\left(\frac{(\chi_i^n)^T \{P(t_{j+1})\}^n_i}{(\chi_i^n)^T m_{ii}^d \chi_i^n}\right)^{0.5}. \qquad (50)$$

where in, $d$ is $u$, $\varphi$, $\psi$ and w also known as freedom degrees of structure, $c_i^n$ is critical damping coefficient at $i^{th}$ spatial node, $\tau^n$ depicts fictitious incremental time which is generally taken as unity and the element of the stiffness matrix is determined as $k_{il}$. To calculate the stiffness matrix, we have:

$$K = \frac{\partial\big([K_{j+1}]^n \{\chi_{j+1}\}^n\big)}{\partial \chi}. \qquad (51)$$

in which $\chi = u, \varphi, \psi \text{ and } w$ are vectors of approximate solution. A set of finite difference statements should be written in order to finalize the iterative procedure by using the acceleration and velocity terms as follows:

$$\ddot{\chi}^n = \left(\frac{\dot{\chi}^{n+0.5} - \dot{\chi}^{n-0.5}}{\tau^n}\right), \qquad (52)$$

$$\dot{\chi}^{n-0.5} = \left(\frac{\chi^n - \chi^{n-1}}{\tau^n}\right). \qquad (53)$$

The velocities at the next time step can be defined as [57]:

$$\dot{\chi}_i^{n+0.5} = \frac{(2m_{ii}^d - \tau^n c_i^n)}{(2m_{ii}^d + \tau^n c_i^n)}\dot{\chi}_i^{n-0.5}$$
$$+ \frac{2\tau^n}{(2m_{ii}^d + \tau^n c_i^n)}(R)^n. \qquad (54)$$

Now out of balance force vector and kinetic energy of the system can be calculated as:

$$(R)^n = \{P(t_{j+1})\}^n - \big[K_{j+1}\big]^n \{\chi_{j+1}\}^n, \qquad (55)$$

$$KE^{n+1} = \sum_{j=1}^{N}\{\dot{\chi}_j^{n+0.5}\}^2. \qquad (56)$$

In each time step by applying integration on velocities, the displacements will be calculated by:

$$\chi^{n+1} = \chi^n + \tau^{n+1}\dot{\chi}^{n+0.5}. \qquad (57)$$

The V-DR process is continued with iterative steps to fulfill desired convergence criteria, i.e., $KE^{n+1} \leq 10^{-12}$ and $(R)^n \leq 10^{-6}$. The following flowchart (Fig. 4) explains the V-DR method in combination with the Newmark direct integration technique:
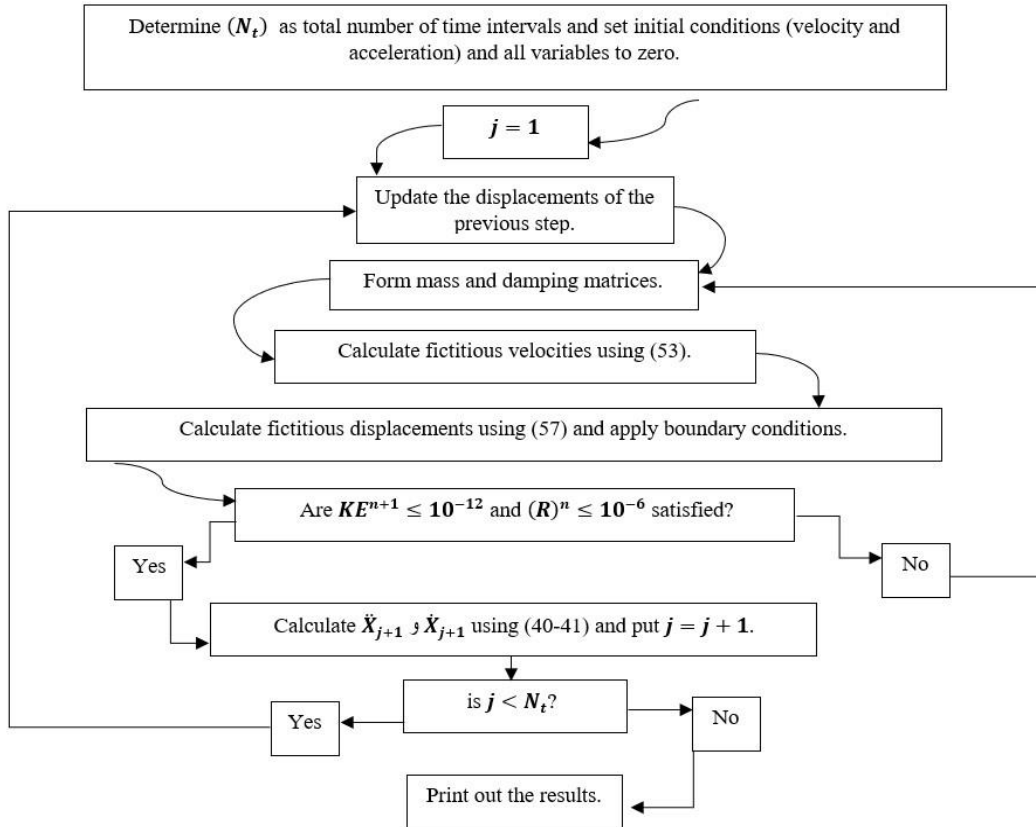
**Fig. 4.** Newmark direct integration in combination with the Dynamic relaxation method

## 5. Numerical Results

### 5.1. Validation

As a first example to prove the accuracy of the present study in this section, the maximum deflection of a circular FG plate based on FSDT is compared with those of Reddy *et al.* [58]. The plate is subjected to a uniform distributed load with clamped and simply supported boundary conditions. The effect of different power law indices with three thickness-to-radius ratios are presented in the following. The material properties and uniform load which are used in this example are:

$$\bar{q} = F_0 r_o^4 / E_m h^4,$$

$$W_{max} = 64 w D_c / F_0 r_o^4,$$

$$D_c = E_c h^3 / 12(1 - v^2),$$

$$F_0 = 0.14 \; Gpa,$$

$$v = 0.288,$$

$$E_c = 151.0 \; Gpa,$$

$$E_m / E_c = 0.396. \tag{58}$$

Tables 1 and 2 show the great consistency of the viscous damping DR method with those gained by Reddy *et al.* [58].

**Table 1.** Comparison of nondimensional maximum deflection in simply supported condition with Ref. [58]

Thickness radius ratio, $h/r_o$

| | Reddy *et al.* [58] | | | Present study | | |
|---|---|---|---|---|---|---|
| n | 0.1 | 0.15 | 0.2 | 0.1 | 0.15 | 0.2 |
| 0 | 10.481 | 10.623 | 10.822 | 10.469 | 10.623 | 10.820 |
| 2 | 5.539 | 5.610 | 5.708 | 5.534 | 5.609 | 5.706 |
| 4 | 5.153 | 5.217 | 5.307 | 5.155 | 5.219 | 5.308 |
| 8 | 4.810 | 4.870 | 4.954 | 4.810 | 4.864 | 4.955 |
| 10 | 4.712 | 4.772 | 4.855 | 4.711 | 4.764 | 4.857 |
| 50 | 4.291 | 4.338 | 4.428 | 4.286 | 4.338 | 4.430 |
| 100 | 4.223 | 4.280 | 4.359 | 4.220 | 4.278 | 4.358 |
| 1000 | 4.158 | 4.214 | 4.293 | 4.155 | 4.218 | 4.292 |
| 10e05 | 4.151 | 4.207 | 4.285 | 4.150 | 4.204 | 4.285 |

**Table 2.** Comparison of nondimensional maximum deflection in clamped supported condition with Ref. [58]

| | | | | | | |
|---|---|---|---|---|---|---|
| Thickness radius ratio, $h/r_o$ | | | | | | |
| | Reddy *et al.* [58] | | | Present study | | |
| n | 0.1 | 0.15 | 0.2 | 0.1 | 0.15 | 0.2 |
| 0 | 2.639 | 2.781 | 2.979 | 2.635 | 2.778 | 2.971 |
| 2 | 1.444 | 1.515 | 1.613 | 1.441 | 1.511 | 1.614 |
| 4 | 1.320 | 1.384 | 1.473 | 1.317 | 1.374 | 1.476 |
| 8 | 1.217 | 1.278 | 1.362 | 1.215 | 1.275 | 1.360 |
| 10 | 1.190 | 1.250 | 1.333 | 1.188 | 1.240 | 1.333 |
| 50 | 1.080 | 1.137 | 1.216 | 1.078 | 1.134 | 1.219 |
| 100 | 1.063 | 1.119 | 1.199 | 1.054 | 1.118 | 1.198 |
| 1000 | 1.047 | 1.103 | 1.182 | 1.048 | 1.107 | 1.182 |
| 10e05 | 1.045 | 1.101 | 1.180 | 1.042 | 1.101 | 1.180 |

For a second example to prove the validity and precision of the Newmark integration method, the results of forced vibration analysis under impulsive loading with simply supported boundary conditions are compared with those reported by Ref. [59]. Since there is no evidence based on dynamic analysis of annular FG sandwich porous plates reinforced by graphene platelets in open literature, the following sample is presented in which the plate is degraded into a single layer FG annular plate conforming a power-law function with varying Poisson's ratio based on Mori-Tanaka scheme through different material grading indices whose material properties are:

$$E_m = 70Gpa,$$
$$\nu_m = 0.3,$$
$$\rho_m = 2702 \, kg/m^3,$$
$$E_c = 427Gpa,$$
$$\nu_c = 0.17,$$
$$\rho_c = 3100 \, kg/m^3. \tag{59}$$

Figure 5 shows normalized nondimensional deflection $\frac{w}{h}$ at normalized radius point $R = \frac{(r_o + r_i)}{2}$ versus nondimensional time $T = \frac{t}{\Delta t}$ with $\Delta t = 0.01$. The results show the efficiency and accuracy of the procedure and are found to be in great consistency with the analytical solution of Ref. [59].
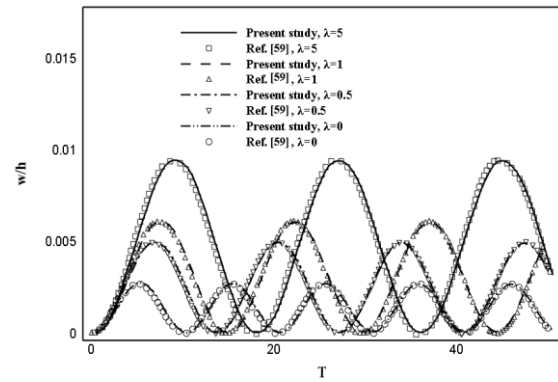


**Fig. 5.** Comparison study for the dynamic behavior of simply supported FG annular plate with different power law indices under impulsive loading. $r_o/h = 6, r_i/h = 3,$ $F(t) = q_0 = 0.42Gpa, (t < \infty)$

To carry out the convergence study to state the number of spatial nodes, the following results are achieved for both boundary conditions based on FSDT and MHSDT. For instance, non-dimensional deflection of clamped-clamped porous GPL reinforced annular plate under an impulsive loading $(q_0 = 500kpa, t < \infty)$ is illustrated in Fig. 6 in terms of time for different node numbers. From the results, the 40 and 30 nodes for FSDT and MHSDT, respectively, are considered for the analysis of the entire process because their responses have acceptable precision with suitable time of analysis.
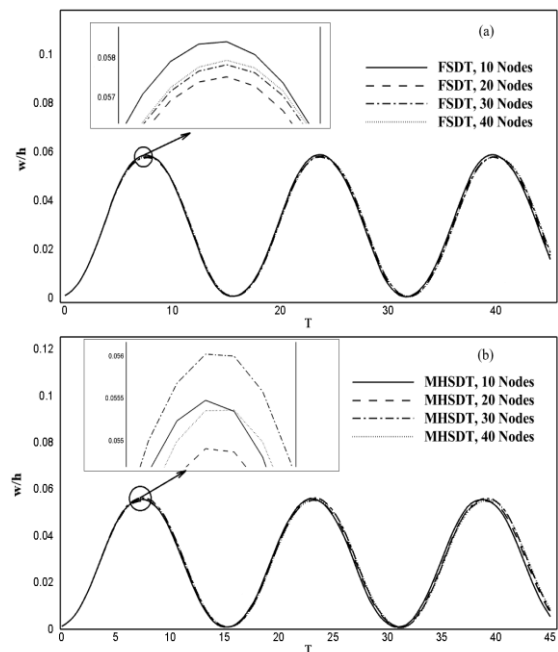


**Fig. 6.** Illustrations of the number of spatial nodes with GPL distribution A, Porosity dispersion II and $W_{gpl} = 1 \, wt.$ %, $e_0 = 0.2, h/r_o = 0.15$ for (a) FSDT and (b) MHSDT

It is noticed that the same number of nodes are used for simply supported conditions with $h/r_o = 0.3$ and different GPL distributions, porosity coefficients, and loadings. From Fig. 6

and similar analyses for convergence study, it can be concluded that modified-higher order theory can achieve more efficient and accurate results with fewer number of nodes.

## 5.2. Parametric Study

This section is devoted to investigating the influence of some substantial factors namely porosity dispersion and coefficients, GPL distribution and weight fractions, aspect ratio, and boundary conditions under two types of loadings on dynamic results of the GPL-reinforced porous FGM annular sandwich plate. The isotropic face sheets are assumed to be completely interconnected with the porous core and have the same properties as the metallic matrix of the core. Implemented material properties of the sandwich plate are taken from [49] shown in Table 3:

**Table 3.** The material property of GPL-reinforced porous core and isotropic face sheets [49]

| | Elasticity moduli (Gpa) | Density (Kg/m³) | Poisson's ratio |
|---|---|---|---|
| GPL (core) | 1010 | 1062.5 | 0.186 |
| Aluminum (Face sheets and metallic matrix) | 68.3 | 2689.8 | 0.34 |

To carry out the parametric study, an annular graphene platelet reinforced porous sandwich plate with different aspect ratios and geometric parameters with $h/r_o = 0.3$ ($h_c = 0.02m$, $h_f = 0.005m$) and $h/r_o = 0.15$ ($h_c = 0.01m$, $h_f = 0.0025m$), $r_0 = 0.1m$ and $r_i = 0.02m$ are assumed in this section. Also, two types of loadings, an impact, and a simple harmonic excitation, are applied on the upper surface of the sandwich plate as follows:

$$Impact\ loading\ F(t) = \begin{cases} q_0 t, t \le t_p \\ 0, t > t_p \end{cases}, \qquad (60)$$

$$Harmonic\ excitation\ F(t) = q_0 sin(20)t, t < \infty. \qquad (61)$$

For all cases, the non-dimensional dynamic deflections are computed with the following loading specifications at normalized point R which are defined below:

$$R = \frac{(r_o + r_i)}{2},$$
$$T = \frac{t}{\Delta t},$$
$$t_p = 0.3,$$
$$q_0 = 500kpa. \qquad (62)$$

Also, the GPL parameters are taken as $l_{gpl} = 2.5\mu m$, $w_{gpl} = 1.5\mu m$ and $t_{gpl} = 1.5nm$.

The effect of thickness-to-radius ratio for the FSDT and MHSDT subjected to an impact loading with S-S and C-C boundary conditions and $\Delta t = 0.004$ are illustrated in figures 7 and 8 for impact and harmonic loadings, respectively. As shown in Figures 7 and 8, the difference between FSDT and MHSDT becomes greater as the thickness of the FG sandwich annular plate is increased. One reason for this occurrence is the lack of accuracy in FSDT for thicker plates due to the consideration of shear strain as linear, hence with higher-order displacement fields, one can achieve displacements with higher accuracy. Also, it can be observed that the mentioned differences are more noticeable in S-S boundary conditions compared to C-C ones.
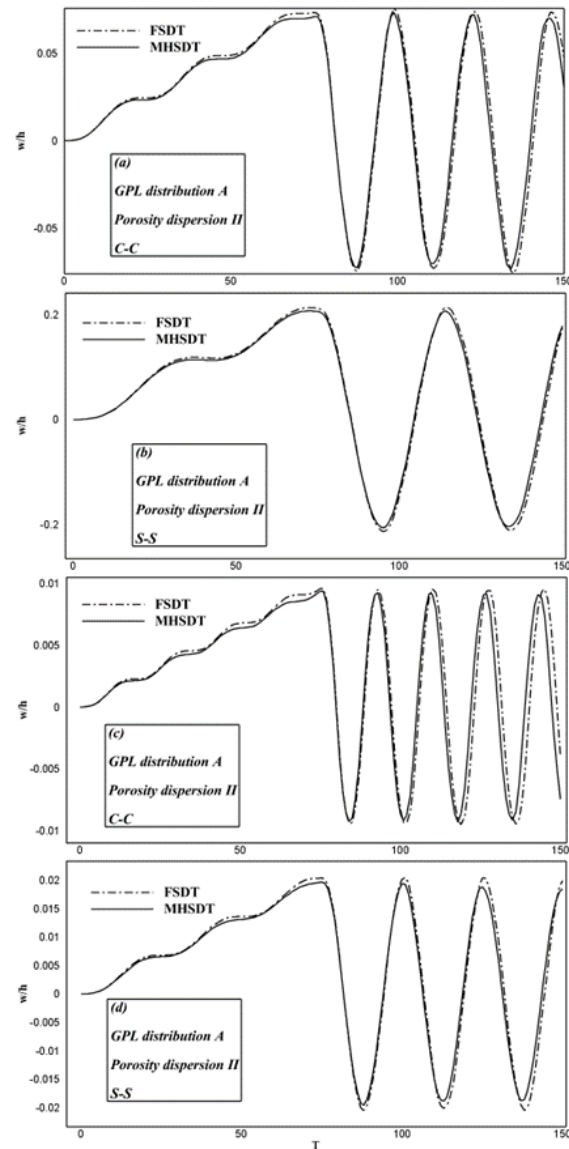


**Fig. 7.** Effects of aspect ratio on the dynamic behavior of sandwich annular plate subjected to impact loading with $e_0 = 0.2$, $W_{gpl} = 0.5\ wt.\%$, for (a), (b) $\{h/r_o = 0.15\}$ and (c), (d) $\{h/r_o = 0.3\}$
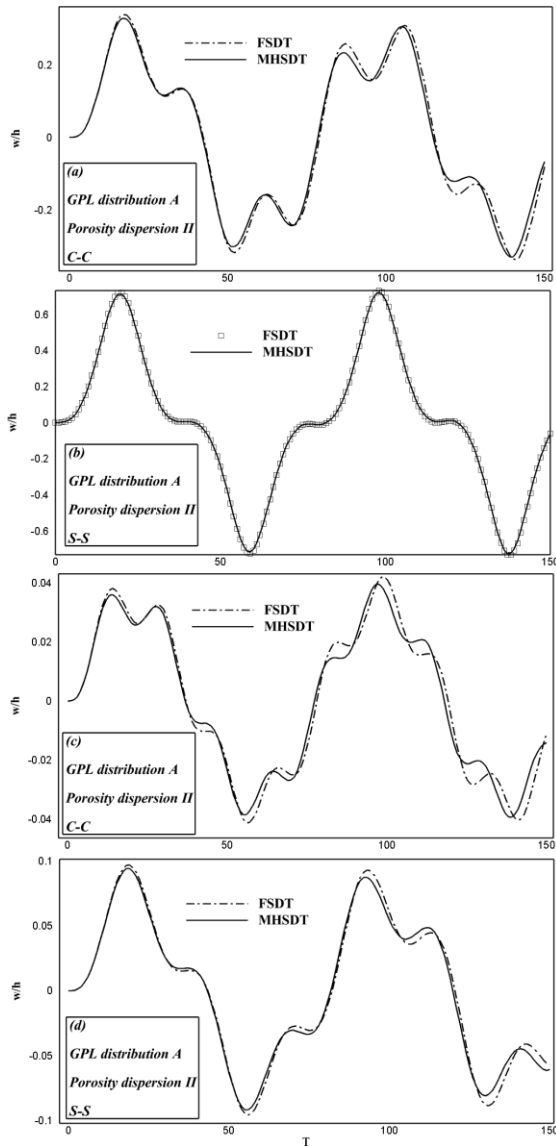
**Fig. 8.** Effects of aspect ratio on the dynamic behavior of sandwich annular plate subjected to harmonic loading with $e_0 = 0.2, W_{gpl} = 0.5\, wt.\%$, for (a), (b)$\left\{{}^h\!/_{r_o} = 0.15\right\}$ and (c), (d) $\left\{{}^h\!/_{r_o} = 0.3\right\}$
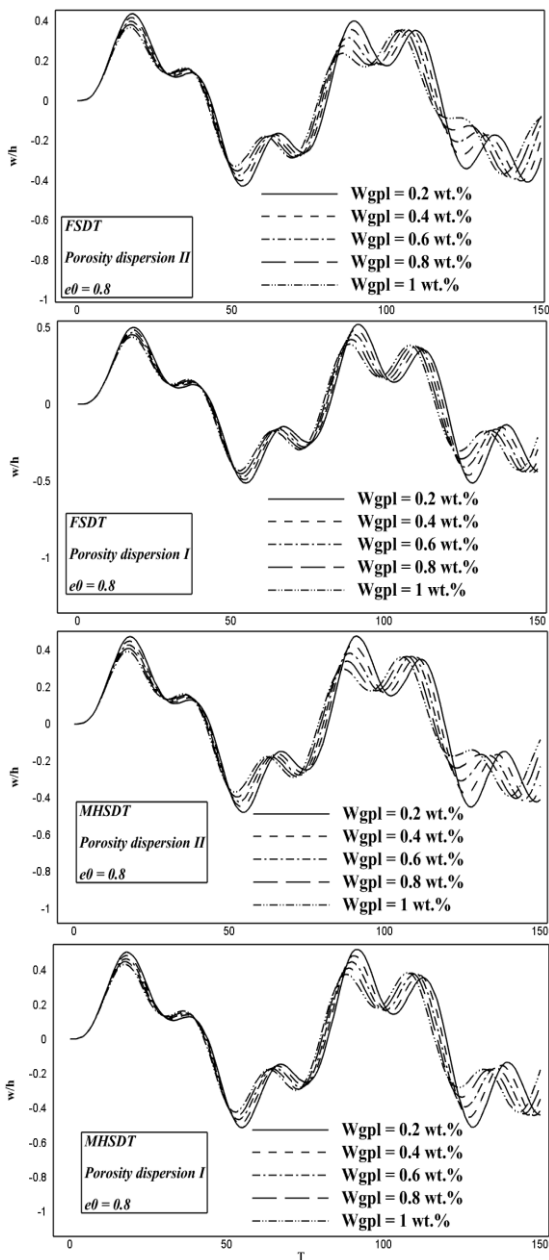
Nondimensional deflection versus dimensionless time ($\Delta t = 0.004$) for two graphene distributions A and B with different porosity dispersions namely I and II under impact and harmonic loadings are shown in figures 9 and 10, respectively. As seen in Figures 9 and 10, the effect of weight fraction $wt.\%$ on the dynamic behavior of sandwich porous plate is also considered for both theories of MHSDT and FSDT with different thickness-to-radius ratios and boundary conditions. As shown in Fig. 9, adding $0.8\, wt.\%$ to the porous core of the sandwich plate, the flexural rigidity will increase with the addition of $0.8\, wt.\%$ to the porous core of sandwich plate, the flexural rigidity will increase significantly, for instance, this increase is about 27.2% for porosity dispersion II in FSDT and 25% in MHSDT. Similarly, using porosity

dispersion I, this increase is about 14.2% and 14.8% for FSDT and MHSDT, respectively. As illustrated in Fig. 10 for GPL distribution B and clamped-clamped supported porous sandwich annular plate with h/r_o =0.15 under a harmonic loading, with the addition of only 0.8 wt.% to the porous plate, an increase in bending rigidity is observed. In this case, the values of 16.2% and 13.6% are seen for dispersions II and I in FSDT and the ones of 17.9% and 13.9%, respectively, in MSHDT. Also, as observed by adding more GPL to the porous core leads to a great decrease in the amplitude of vibrational waves of the whole structure in which the results for MHSDT are observed to be more accurate amongst the FSDTs by revealing more stable peak point kinetic energy at the end of each Dynamic Relaxation algorithm. Furthermore, as figures 9 and 10 illustrate, for thicker plates, porosity dispersion II combined with GPL distributions A and B reveal higher deflection changes in the maximum porosity coefficient between MHSDT and FSDT. The greater the porosity coefficient, the more reduction in the stiffness of the plate, therefore the following particularly discusses the effect of the porosity coefficient on the dynamic history of porous sandwich annular plate reinforced by graphene platelets.
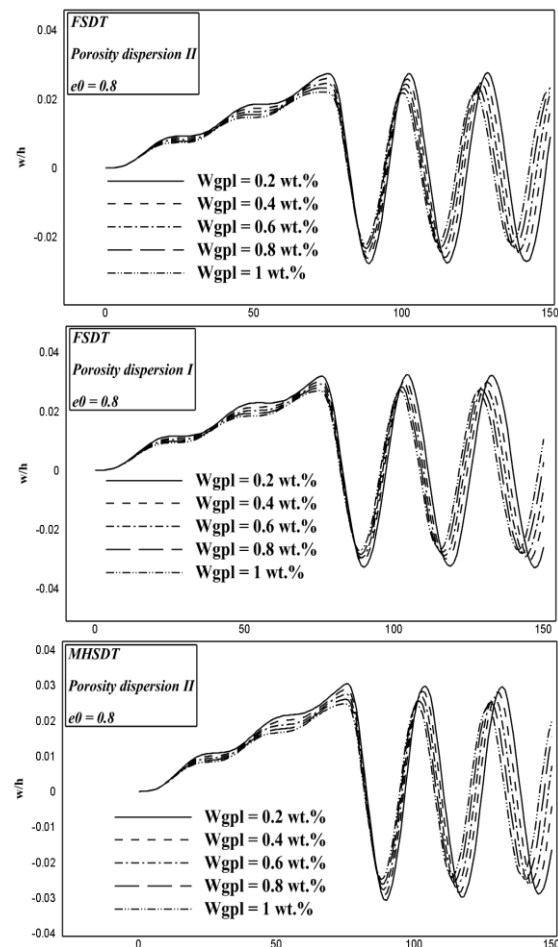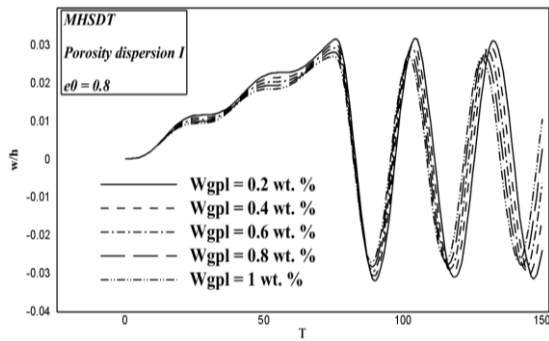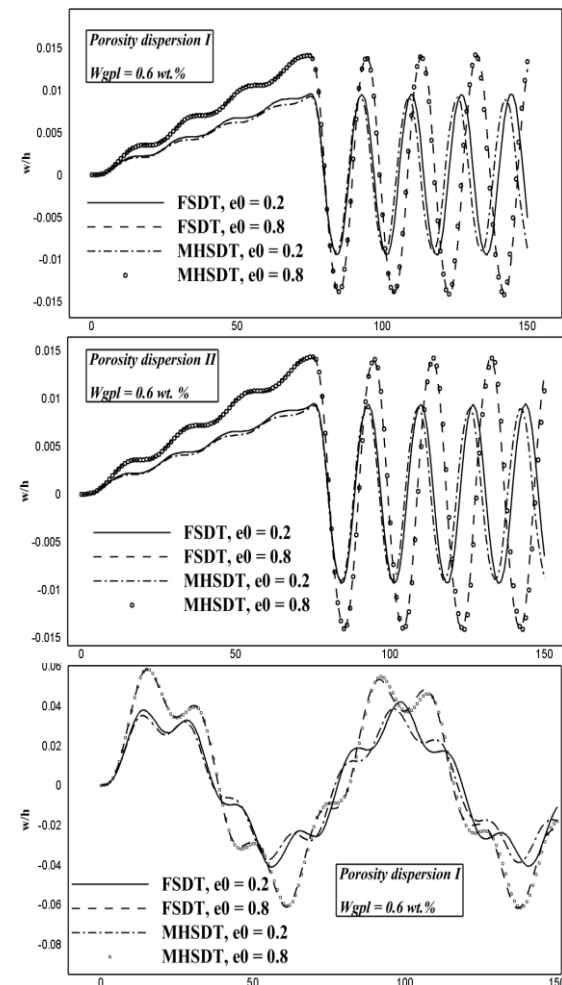
**Fig. 9.** Effect of GPL weight fraction on the dynamic behavior of an S-S edged porous sandwich plate subjected to an impact loading using graphene distribution A with $h/r_o = 0.3$



Figure 11 shows the dynamic behavior of a C-C edged porous sandwich plate subjected to impact and harmonic loadings in graphene distribution A and porosity dispersions I, II with $h/r_o = 0.3$ based on both FSDT and MHSDT. The GPL weight fraction is considered a constant amount of 0.6% in this section and the porosity coefficient is changing from 0.2 to 0.8. The stiffness of the plate shows better reinforcement behavior in graphene distribution A combined with porosity dispersion II as the porosity coefficient greatens.

Figure 12 discusses the dynamic response of an S-S conditioned graphene-reinforced sandwich annular plate under impact loading with $h/r_o = 0.15$ based on both theories with GPL distribution B and porosity distributions I and II. It shows that the same as clamped boundary conditions, the porosity dispersion II has a bigger influence on the strengthening of the porous core in simply supported conditions. Comparing the time history results in figures 7 to 12 with respect to the strength reinforcing of the plates leads to the following best order of composition of porosity and GPL distributions which is (GPL A-Porosity II), (GPL B-porosity II), (GPL A-Porosity II) and (GPL B-Porosity I).
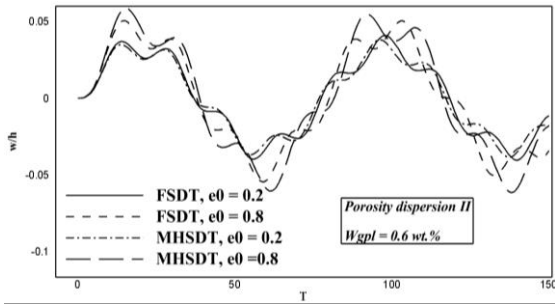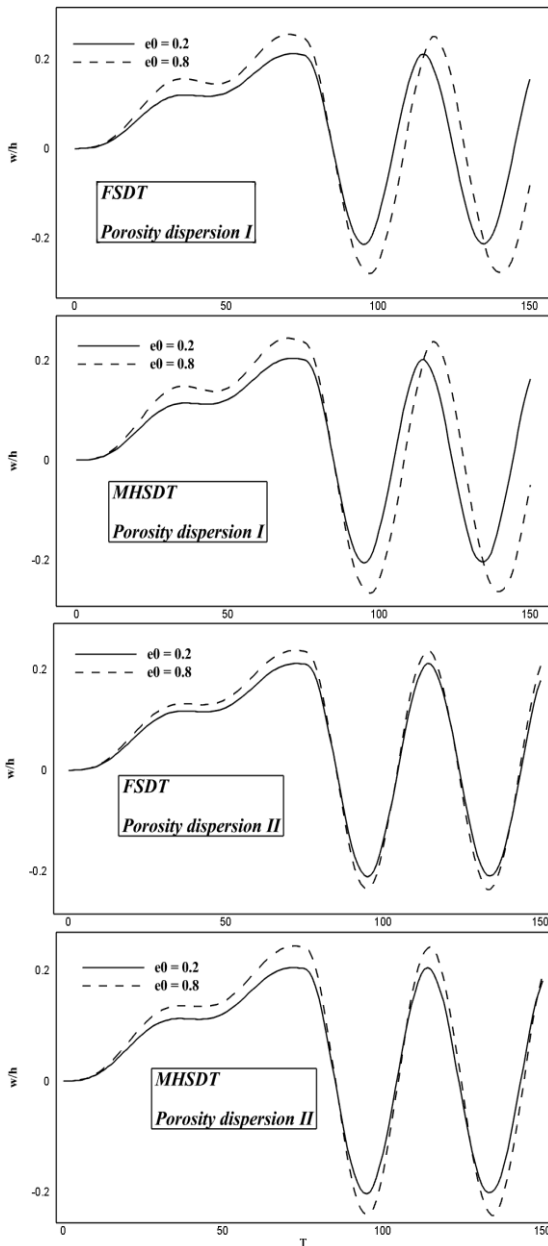


**Fig. 10.** Effect of GPL weight fraction on dynamic behavior of a C-C edged porous sandwich plate subjected to a harmonic loading using graphene distribution B with $h/r_o = 0.15$

**Fig. 11.** Effect of porosity on the dynamic behavior of a C-C-edged porous sandwich plate subjected to impact and harmonic loadings with graphene distribution A and $h/r_o = 0.3$



**Fig. 12.** Effect of porosity on the dynamic behavior of an S-S-edged porous sandwich plate subjected to an impact loading with graphene distribution B and $h/r_o = 0.15$

Ultimately, in order to assess the relative efficacy of each combined GPL and porosity pattern, the outcomes of an impulsive loading on the plate are presented in Figure 13. The figure demonstrates that the optimal reinforcement capacity is achieved through the implementation of GPL distribution A in conjunction with porosity dispersion II.
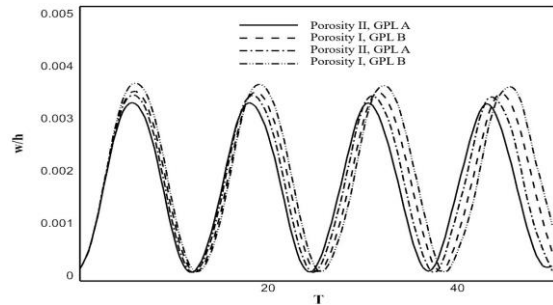


**Fig. 13.** Effect of GPL distributions and porosity patterns in terms of time history for C-C edged porous sandwich plate with $h/r_o = 0.3$

## 6. Conclusions and Remarks

This paper investigates the dynamic analysis of annular functionally graded porous GPL-reinforced sandwich plates based on both MHSDT and FSDT and different boundary conditions. According to closed-cell cellular solids with Gaussian Random Field and Halpin-Tsai micromechanics, the effective material properties of the porous core are developed. The Newmark direct integration technique in combination with the viscous Dynamic Relaxation method is applied to solve time-dependent equations of motion. In fact, the primary and innovative aspect of this approach lies in the combination of the viscous dynamic relaxation method with the Newmark integration method, which has not been previously employed in the literature for sandwich structures. Additionally, the utilization of the modified higher-order shear deformation theory, two graphene distributions, and two porosity dispersions containing various GPL weight fractions and pore coefficients are considered for the porous core. Considering the dynamic behavior of porous sandwich plates under impact and harmonic loads with S-S and C-C boundary conditions and different aspect ratios, some remarkable points are concluded as follows:

- An increase of more than 27 % in plate stiffness is observed by adding only 0.8 wt.% GPL to the porous core of the sandwich plate.

- Both symmetric (II) and asymmetric (I) porosity dispersions play a significant role in the dynamic behavior of the plate, however symmetric porosity dispersion (II) owns the most influence in deflection decrease. Also, among GPL distributions A and B, the non-uniform symmetric graphene distribution A acts as the best strengthener pattern.

- A combination of (GPL A-Porosity II), (GPL B-porosity II), (GPL A-Porosity II), and (GPL B-Porosity I), respectively, leads to the best order of strength reinforcing results for the plates.

- With an increase in porosity, the difference between the results of FSDT and MHSDT greatens.

## Conflicts of Interest

The author declares that there is no conflict of interest regarding the publication of this manuscript.

## References

[1] Beskos, D. & Leung, K., 1984. Dynamic response of plate systems by combining finite differences, finite elements and laplace transform. *Computers & structures, 19* (5-6), pp.763-775.

[2] Nath, Y., Dumir, P. & Bhatiaf, R., 1985. Nonlinear static and dynamic analysis of circular plates and shallow spherical shells using the collocation method. *International journal for numerical methods in engineering, 21* (3), pp.565-578.

[3] Smaill, J., 1990. Dynamic response of circular plates on elastic foundations: Linear and non-linear deflection. *Journal of sound and vibration, 139* (3), pp.487-502.

[4] Srinivasan, R. & Ramachandra, L., 1990. Axisymmetric nonlinear dynamic response of bimodulus annular plates.

[5] Shen, W.Q. & Jones, N., 1993. Dynamic response and failure of fully clamped circular plates under impulsive loading. *International journal of impact engineering, 13* (2), pp.259-278.

[6] Dey, S. & Rao, V.T., 1997. Transient response of circular plates and membranes: A numerical approach. *International journal of mechanical sciences, 39* (12), pp.1405-1413.

[7] Bassi, A., Genna, F. & Symonds, P., 2003. Anomalous elastic–plastic responses to short pulse loading of circular plates. *International Journal of Impact Engineering, 28* (1), pp.65-91.

[8] Peng, J.-S., Yuan, Y.-Q., Yang, J. & Kitipornchai, S., 2009. A semi-analytic approach for the nonlinear dynamic response of circular plates. *Applied Mathematical Modelling, 33* (12), pp.4303-4313.

[9] Aiyesimi, Y., Mohammed, A. & Sadiku, S., 2011. A finite element analysis of the dynamic responses of a thick uniform elastic circular plate subjected to an exponential blast loading. *American Journal of Computational and Applied Mathematics, 1* (2), pp.57-62.

[10] Eipakchi, H. & Khadem Moshir, S., 2020. Dynamic response determination of viscoelastic annular plates using fsdt–perturbation approach. *Journal of Computational Applied Mechanics, 51* (1), pp.98-106.

[11] Zenkour, A., 2005. A comprehensive analysis of functionally graded sandwich plates: Part 2—buckling and free vibration. *International Journal of Solids and Structures, 42* (18-19), pp.5243-5258.

[12] Dai, H.-L., Guo, Z.-Y. & Yang, L., 2013. Nonlinear dynamic response of functionally graded materials circular plates subject to low-velocity impact. *Journal of Composite Materials, 47* (22), pp.2797-2807.

[13] Dai, H.-L., Dai, T. & Cheng, S.-K., 2015. Transient response analysis for a circular sandwich plate with an fgm central disk. *Journal of Mechanics, 31* (4), pp.417-426.

[14] Molla-Alipour, M., 2016. Dynamic behavior analysis of fg circular and annular plates with stepped variations of thickness under various load. *Modares Mechanical Engineering, 16* (7), pp.251-260.

[15] Arshid, E. & Khorshidvand, A.R., 2018. Free vibration analysis of saturated porous fg circular plates integrated with piezoelectric actuators via differential quadrature method. *Thin-Walled Structures, 125*, pp.220-233.

[16] Chen, D., Yang, J. & Kitipornchai, S., 2019. Buckling and bending analyses of a novel functionally graded porous plate using chebyshev-ritz method. *Archives of Civil and Mechanical Engineering, 19* (1), pp.157-170.

[17] Cuong-Le, T., Nguyen, K.D., Nguyen-Trong, N., Khatir, S., Nguyen-Xuan, H. & Abdel-Wahab, M., 2021. A three-dimensional solution for free vibration and buckling of annular plate, conical, cylinder and cylindrical shell of fg porous-cellular materials using iga. *Composite Structures, 259*, pp.113216.

[18] Daikh, A.A. & Zenkour, A.M., 2019. Effect of porosity on the bending analysis of various functionally graded sandwich plates. *Materials Research Express, 6* (6), pp.065703.

[19] Daikh, A.A. & Zenkour, A.M., 2019. Free vibration and buckling of porous power-law and sigmoid functionally graded sandwich plates using a simple higher-order shear deformation theory. *Materials Research Express, 6* (11), pp.115707.

[20] Fouda, N., El-Midany, T. & Sadoun, A., 2017. Bending, buckling and vibration of a functionally graded porous beam using finite elements. *Journal of applied and computational mechanics, 3* (4), pp.274-282.

[21] Rahmani, M., Mohammadi, Y. & Kakavand, F., 2019. Vibration analysis of different types of porous fg circular sandwich plates. *ADMT Journal, 12* (3)**,** pp.63-75.

[22] Babaei, M., Hajmohammad, M.H. & Asemi, K., 2020. Natural frequency and dynamic analyses of functionally graded saturated porous annular sector plate and cylindrical panel based on 3d elasticity. *Aerospace Science and Technology, 96***,** pp.105524.

[23] Esmaeilzadeh, M., Golmakani, M. & Sadeghian, M., 2020. A nonlocal strain gradient model for nonlinear dynamic behavior of bi-directional functionally graded porous nanoplates on elastic foundations. *Mechanics Based Design of Structures and Machines***,** pp.1-20.

[24] Akbaş, Ş., Fageehi, Y., Assie, A. & Eltaher, M., 2020. Dynamic analysis of viscoelastic functionally graded porous thick beams under pulse load. *Engineering with Computers***,** pp.1-13.

[25] Kitipornchai, S., Chen, D. & Yang, J., 2017. Free vibration and elastic buckling of functionally graded porous beams reinforced by graphene platelets. *Materials & Design, 116***,** pp.656-665.

[26] Chen, D., Yang, J. & Kitipornchai, S., 2017. Nonlinear vibration and postbuckling of functionally graded graphene reinforced porous nanocomposite beams. *Composites Science and Technology, 142***,** pp.235-245.

[27] Yang, J., Chen, D. & Kitipornchai, S., 2018. Buckling and free vibration analyses of functionally graded graphene reinforced porous nanocomposite plates based on chebyshev-ritz method. *Composite Structures, 193***,** pp.281-294.

[28] Polit, O., Anant, C., Anirudh, B. & Ganapathi, M., 2019. Functionally graded graphene reinforced porous nanocomposite curved beams: Bending and elastic stability using a higher-order model with thickness stretch effect. *Composites Part B: Engineering, 166***,** pp.310-327.

[29] Li, Q., Wu, D., Chen, X., Liu, L., Yu, Y. & Gao, W., 2018. Nonlinear vibration and dynamic buckling analyses of sandwich functionally graded porous plate with graphene platelet reinforcement resting on winkler–pasternak elastic foundation. *International Journal of Mechanical Sciences, 148***,** pp.596-610.

[30] Esmaeilzadeh, M. & Kadkhodayan, M., 2019. Numerical investigation into dynamic behaviors of axially moving functionally graded porous sandwich nanoplates reinforced with graphene platelets. *Materials Research Express, 6* (10)**,** pp.1050b7.

[31] Safarpour, M., Rahimi, A., Alibeigloo, A., Bisheh, H. & Forooghi, A., 2019. Parametric study of three-dimensional bending and frequency of fg-gplrc porous circular and annular plates on different boundary conditions. *Mechanics Based Design of Structures and Machines***,** pp.1-31.

[32] Rahimi, A., Alibeigloo, A. & Safarpour, M., 2020. Three-dimensional static and free vibration analysis of graphene platelet–reinforced porous composite cylindrical shell. *Journal of Vibration and Control, 26* (19-20)**,** pp.1627-1645.

[33] Zhao, S., Yang, Z., Kitipornchai, S. & Yang, J., 2020. Dynamic instability of functionally graded porous arches reinforced by graphene platelets. *Thin-Walled Structures, 147***,** pp.106491.

[34] Nguyen, L.B., Nguyen, N.V., Thai, C.H., Ferreira, A. & Nguyen-Xuan, H., 2019. An isogeometric bézier finite element analysis for piezoelectric fg porous plates reinforced by graphene platelets. *Composite Structures, 214***,** pp.227-245.

[35] Arshid, E., Amir, S. & Loghman, A., 2020. Static and dynamic analyses of fg-gnps reinforced porous nanocomposite annular micro-plates based on msgt. *International Journal of Mechanical Sciences, 180***,** pp.105656.

[36] Gao, W., Qin, Z. & Chu, F., 2020. Wave propagation in functionally graded porous plates reinforced with graphene platelets. *Aerospace Science and Technology, 102***,** pp.105860.

[37] Nejadi, M., Mohammadimehr, M. & Mehrabi, M., 2021. Free vibration and stability analysis of sandwich pipe by considering porosity and graphene platelet effects on conveying fluid flow. *Alexandria Engineering Journal, 60* (1)**,** pp.1945-1954.

[38] Tao, C. & Dai, T., 2021. Isogeometric analysis for postbuckling of sandwich cylindrical shell panels with graphene platelet reinforced functionally graded porous core. *Composite Structures, 260***,** pp.113258.

[39] Khayat, M., Baghlani, A. & Najafgholipour, M., 2021. The propagation of uncertainty in the geometrically nonlinear responses of smart sandwich porous cylindrical shells reinforced with graphene platelets. *Composite Structures, 258***,** pp.113209.

[40] Nguyen, N.V., Lee, J. & Nguyen-Xuan, H., 2019. Active vibration control of gpls-reinforced fg metal foam plates with piezoelectric sensor and actuator layers. *Composites Part B: Engineering, 172***,** pp.769-784.

[41] Nguyen, N.V., Nguyen, L.B., Nguyen-Xuan, H. & Lee, J., 2020. Analysis and active control of

geometrically nonlinear responses of smart fg porous plates with graphene nanoplatelets reinforcement based on bézier extraction of nurbs. *International Journal of Mechanical Sciences, 180*, pp.105692.

[42] Nguyen, N.V., Nguyen-Xuan, H., Lee, D. & Lee, J., 2020. A novel computational approach to functionally graded porous plates with graphene platelets reinforcement. *Thin-Walled Structures, 150*, pp.106684.

[43] Nguyen, N.V. & Lee, J., 2021. On the static and dynamic responses of smart piezoelectric functionally graded graphene platelet-reinforced microplates. *International Journal of Mechanical Sciences, 197*, pp.106310.

[44] Nguyen, N.V., Phan, D.-H. & Lee, J., 2022. Nonlinear static and dynamic isogeometric analysis of functionally graded microplates with graphene-based nanofillers reinforcement. *Aerospace Science and Technology, 127*, pp.107709.

[45] Nguyen, N.V., Phan, D.-H. & Lee, J., 2023. On the transient performance of agglomerated graphene platelets-reinforced porous sandwich plates. *Thin-Walled Structures, 183*, pp.110316.

[46] Barati, M.R. & Zenkour, A.M., 2019. Analysis of postbuckling of graded porous gpl-reinforced beams with geometrical imperfection. *Mechanics of Advanced Materials and Structures, 26* (6), pp.503-511.

[47] Gao, K., Gao, W., Chen, D. & Yang, J., 2018. Nonlinear free vibration of functionally graded graphene platelets reinforced porous nanocomposite plates resting on elastic foundation. *Composite Structures, 204*, pp.831-846.

[48] Ansari, R., Hassani, R., Gholami, R. & Rouhi, H., 2020. Nonlinear bending analysis of arbitrary-shaped porous nanocomposite plates using a novel numerical approach. *International Journal of Non-Linear Mechanics, 126*, pp.103556.

[49] Li, K., Wu, D., Chen, X., Cheng, J., Liu, Z., Gao, W. & Liu, M., 2018. Isogeometric analysis of functionally graded porous plates reinforced by graphene platelets. *Composite Structures, 204*, pp.114-130.

[50] Roberts, A. & Garboczi, E.J., 2002. Computation of the linear elastic properties of random porous materials with a wide variety of microstructure. *Proceedings of the Royal Society of London. Series A: Mathematical, Physical and Engineering Sciences, 458* (2021), pp.1033-1054.

[51] Dong, Y., Li, Y., Chen, D. & Yang, J., 2018. Vibration characteristics of functionally graded graphene reinforced porous nanocomposite cylindrical shells with spinning motion. *Composites Part B: Engineering, 145*, pp.1-13.

[52] Barati, M.R. & Zenkour, A.M., 2019. Vibration analysis of functionally graded graphene platelet reinforced cylindrical shells with different porosity distributions. *Mechanics of Advanced Materials and Structures, 26* (18), pp.1580-1588.

[53] Nguyen, Q.H., Nguyen, L.B., Nguyen, H.B. & Nguyen-Xuan, H., 2020. A three-variable high order shear deformation theory for isogeometric free vibration, buckling and instability analysis of fg porous plates reinforced by graphene platelets. *Composite Structures, 245*, pp.112321.

[54] Dastjerdi, S., Abbasi, M. & Yazdanparast, L., 2017. A new modified higher-order shear deformation theory for nonlinear analysis of macro-and nano-annular sector plates using the extended kantorovich method in conjunction with sapm. *Acta Mechanica, 228* (10), pp.3381-3401.

[55] Dastjerdi, S. & Abbasi, M., 2020. A new approach for time-dependent response of viscoelastic graphene sheets embedded in visco-pasternak foundation based on nonlocal fsdt and mhsdt theories. *Mechanics of Time-Dependent Materials, 24* (3), pp.329-361.

[56] Golmakani, M. & Kadkhodayan, M., 2011. Nonlinear bending analysis of annular fgm plates using higher-order shear deformation plate theories. *Composite Structures, 93* (2), pp.973-982.

[57] Rezaiee-Pajand, M., Alamatian, J. & Rezaee, H., 2017. The state of the art in dynamic relaxation methods for structural mechanics part 1: Formulations. *Iranian Journal of Numerical Analysis and Optimization, 7* (2), pp.65-86.

[58] Reddy, J., Wang, C. & Kitipornchai, S., 1999. Axisymmetric bending of functionally graded circular and annular plates. *European Journal of Mechanics-A/Solids, 18* (2), pp.185-199.

[59] Eshraghi, I. & Dag, S. 2020. Forced vibrations of functionally graded annular and circular plates by domain-boundary element method. Wiley Online Library.